ACSNANO

www.acsnano.org

ARTICLE

SynCells: A 60 × 60 μm^2 Electronic Platform with Remote Actuation for Sensing Applications in Constrained Environments

Marek Hempel, Vera Schroeder, Chibeom Park, Volodymyr B. Koman, Mantian Xue, Elaine McVay, Sarah Spector, Madan Dubey, Michael S. Strano, Jiwoong Park, Jing Kong, and Tomás Palacios*

Cite This: *ACS Nano* 2021, 15, 8803–8812

Read Online

ACCESS | Metrics & More | Article Recommendations | Supporting Information

ABSTRACT: Autonomous electronic microsystems smaller than the diameter of a human hair (<100 μm) are promising for sensing in confined spaces such as microfluidic channels or the human body. However, they are difficult to implement due to fabrication challenges and limited power budget. Here we present a 60 × 60 μm electronic microsystem platform, or SynCell, that overcomes these issues by leveraging the integration capabilities of two-dimensional material circuits and the low power consumption of passive germanium timers, memory-like chemical sensors, and magnetic pads. In a proof-of-concept experiment, we magnetically positioned SynCells in a microfluidic channel to detect putrescine. After we extracted them from the channel, we successfully read out the timer and sensor signal, the latter of which can be amplified by an onboard transistor circuit. The concepts developed here will be applicable to microsystems targeting a variety of applications from microfluidic sensing to biomedical research.

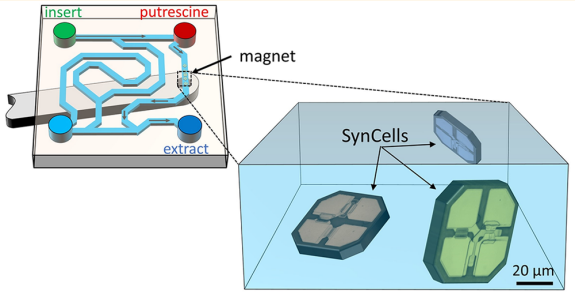

KEYWORDS: *2D materials, MoS_2, magnetic actuation, microfluidics, chemical sensing*

Sensing in spatially constrained environments is highly relevant in areas such as microfluidics and biomedical research. For example, in microfluidic devices sensing is essential for analyzing cells, testing new drugs, or enabling inexpensive home health tests.[1,2] Inside the human body, implantable microscale sensors are currently being investigated for neural and biosensing,[3−5] and sensors as small as red blood cells have been proposed to detect diseases on a cellular level.[6] To address these applications, it is desirable to have micrometer-scale sensors that can be easily deployed and require little infrastructure.

Several strategies have been developed to measure in constrained environments. The most straightforward approach is to reduce the sensor area of a macroscopic setup to attain micrometer sensing resolution, such as silicon-based microelectrodes for neural sensing[7] or embedded sensors in microfluidic systems for bioapplications.[8] However, these techniques can only measure in predefined locations and are wired to larger external supporting equipment. This strongly limits measurement flexibility and makes it difficult to apply these solutions to unstructured environments, such as microfluidic devices without embedded sensors.

Autonomous microsystems are a promising solution for sensing in constrained spaces, offering a high degree of flexibility without external wires. One way such microsystems can be built is by heavily leveraging CMOS integration to miniaturize electronic sensing systems into a single sub-millimeter package, sometimes referred to as Smart Dust.[9,10] Several silicon-based autonomous sensor nodes with sizes down to a few hundred micrometers have been demonstrated, mainly for medical and biosensing applications.[3−5,11−16] However, such systems are still too large to enter microfluidic channels or blood vessels. Designing CMOS-based microsystems below 100 μm in size is exceedingly difficult since complex circuitry such as microcontrollers are no longer feasible even with advanced technology nodes and energy

Received: February 9, 2021
Accepted: May 3, 2021
Published: May 7, 2021

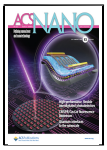

https://doi.org/10.1021/acsnano.1c01259
ACS Nano 2021, 15, 8803–8812

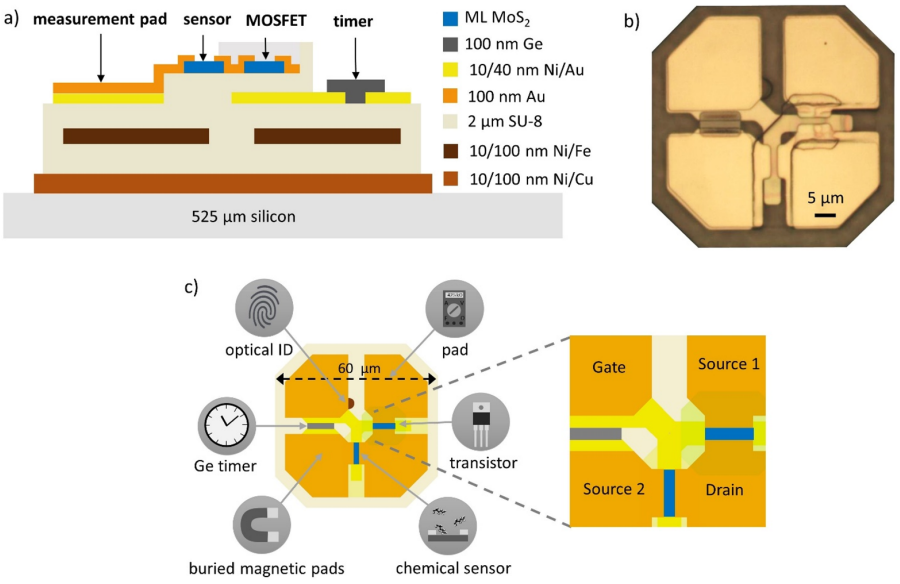

Figure 1. SynCell concept and structure. (a) Cross-section schematic of a "Hybrid SynCell". The SynCells are built on silicon with a 10/100 nm layer of Ni/Cu film as sacrificial release layer. In total, the SynCells consist of nine layers, all patterned by photolithography. (b) Micrograph image of a SynCell. (c) Top-view schematic of a SynCell with MoS_2-based transistors and chemical sensor, Ge-based timer, buried iron pads for magnetic actuation, optical ID tag, and measurement pads for evaluation, with optical image shown in (b).

available from storage or harvesting elements is severely limited to a few microwatts at best.[3,16,17]

To reduce the size below 100 μm, autonomous microsystems with strongly reduced functionality have been proposed, such as sprayable 2D-material microsystems for environmental sensing[17] or optical sensors[18,19] and μtags[20] for biosensing. These approaches sometimes use functional materials that achieve tasks without electric components and simplify the microsystem design. However, all these solutions are single sensor systems, mostly just backscattering or fluorescently re-emitting an input signal that needs immediate read-out or requires constant input power. Alternatively, biologically engineered micro- and nanomachines have been demonstrated for sensing[21] with dimensions of about 1−50 μm, making them the smallest engineered microsystems. However, they also require constant imaging to read out the fluorescent or motion-based sensor output. To increase the utility of these microsystems, more functionality at this small footprint is needed. Additionally, not relying on immediate readout or external power during sensing is helpful to increase the range of applications, while adding actuation methods would greatly increase measurement flexibility.

In this work, we present a 60 × 60 × 2 μm^3 autonomous electronic platform that we call Synthetic Cells, or *SynCells*. Our system consists of several components including molybdenum disulfide-based (MoS_2) transistors and chemical sensors, analog timers based on eroding germanium (Ge) films, and magnetic iron pads for actuation. These building blocks represent a broad set of capabilities and enable functions such as signal amplification, sensing, time tracking, and remote actuation, respectively. By leveraging both electronic and functional material devices we propose a passive sensing approach that does not require power or instantaneous communication while sensing. To show their utility in confined spaces, we magnetically positioned SynCells in a microfluidic channel to detect putrescine. After extracting the SynCells from the channel, we read out the timer and sensor signal, the latter of which can be successfully amplified by an onboard transistor circuit to increase their output signal, demonstrating the utility of our SynCells for sensing in constrained environments.

RESULTS/DISCUSSION

Concept. Designing tiny autonomous microsystems has two main challenges: microsystem size and power budget. Microsystems below 100 μm do not have room for complex circuitry, even with state-of-the-art microfabrication technologies. The smallest ARM Cortex M0+ microcontroller, for example, still takes up 0.073 mm^2 of area with a 28 nm CMOS process node,[22] which is 22 times larger than our proposed SynCells. Furthermore, the amount of electric energy that can be stored or harvested on a sub-100 μm microsystem is severely limited. Available microbatteries are still too large[13] to fit on such systems, and their scaled down charge capacity would be prohibitively low (approximately 0.5 nAh for a 50 × 50 × 50 μm^3 battery[13]). Energy harvesting is able to deliver more power to sub-100 μm microsystems under optimum conditions but is still limited to a few microwatts at best.[3,16,17]

In the SynCell platform we addressed the size and power constraints by designing simple and task-specific SynCells to reduce microsystem size and power budget. Rather than adding all functionality onto a single microsystem, we designed multiple types of SynCells with different layouts and functions. This way, a complex task can be addressed through a diversity of SynCell types. Specifically, we fabricated four types of SynCells; see Supporting Figure S1: a *Sensor SynCell* with two chemical sensor designs and a reference device, a *Timer SynCell* with three different timer designs, an *Amplifier SynCell* with two chemical sensors and a differential amplifier for signal

https://doi.org/10.1021/acsnano.1c01259
ACS Nano 2021, 15, 8803−8812

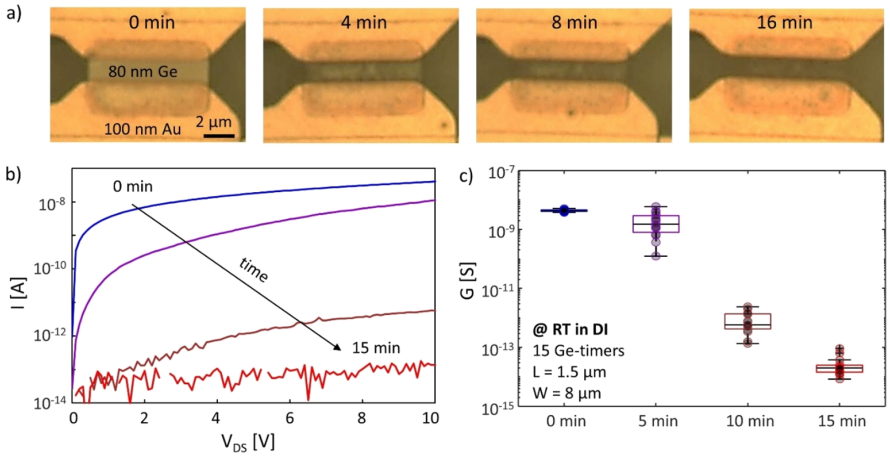

Figure 2. Analysis of germanium-based analog timers. (a) Optical micrographs of a Ge timer after 0, 4, 8, and 16 min of etching in 60 °C warm DI water. (b) Typical current–voltage (*IV*) characteristic of an 80 nm thick Ge timer after 0, 5, 10, and 15 min in room-temperature water. The conductance decreases over time. (c) Timer conductance of 15 timers over time.

conditioning, and a *Hybrid SynCell* with a chemical sensor, an amplifier, and a timer.

To reduce power consumption, all key components of our SynCells operate passively while the SynCells are dispersed in liquid. After exposure to the analyte of interest, the chemiresistive sensors change their conductance and only go back to their original state very slowly, hence also serving as analog memory. The Ge-based timers keep track of time by measuring the oxidation and subsequent erosion of germanium in water.[23] Each SynCell has a 10/100 nm nickel (Ni)/iron (Fe) film embedded inside the SU-8 substrate so that they can to be moved by magnetic fields induced by either moving permanent magnets or changing the current through electromagnets.[24] As a result, the SynCell can travel through hard-to-reach environments and perform different measurements in a fully autonomous manner, without the need of light or other energy sources.

After sensing, the SynCells can be recovered by concentrating them magnetically, drop-casting them on a glass slide, and reading out the sensor and timer thanks to the on-board electronics. Here, built-in transistors on the Amplifier SynCell are used to convert the sensor conductance into a low- or high-voltage signal, depending on whether a chemical exposure occurred. These retrievable and autonomous SynCell microsystems are useful for measuring in confined spaces such as microfluidic channels or distributed piping systems that do not have any infrastructure to provide power or readout sensor values. In the future, the measurement pads could be replaced with an optical communication system to allow direct wireless sensor readout.

The SynCells are built on a Cu/Si sacrificial substrate and are composed of nine layers patterned by photolithography; see Methods and Supporting Information for details. Figure 1a and c show a cross-section and top-view schematic of a "Hybrid SynCell" that contain all building blocks, while a micrograph of the same SynCell is depicted in Figure 1b. Mechanical stability is provided through a 2 μm thin SU-8 polymer film. SU-8 is an ideal substrate material because it is mechanically flexible, chemically inert, biocompatible,[25] and stable at high temperature.[26] On top, thin films of gold, germanium, SU-8, and monolayer MoS_2 grown by metal–organic chemical vapor deposition (MOCVD) are used for the transistors, sensors, analog timers, and measurement pads with the SU-8 also acting as the dielectric layer. MoS_2 was chosen as sensor and transistor materials because it is a high-quality semiconductor and excellent sensing material and can be easily integrated onto an SU-8 substrate at room temperature, as opposed to other electronic thin-film materials. One pad is shaped differently for each SynCell type to create an optical identification (ID) label to distinguish them under the microscope. In total, over 11 300 SynCells are fabricated on each 8 × 8 mm^2 die with a yield above 95% after fabrication based on sampling several hundred SynCells.

SynCell Building Blocks. First, we characterized each SynCell building block separately. For this, the SynCells were fabricated, lifted-off, transferred onto another PMMA/Si carrier, and then tested (see Methods for details).

Germanium Timers. Germanium thin-film timers were used to estimate the time SynCells are submersed in water by leveraging the slow erosion process of Ge in water. In the future, such timers could generate time stamps for sensor data with no additional power or to infer how far SynCells have traveled based on their excursion time. Since germanium is biocompatible in small quantities, it could even be used in biological environments.[27,28] The idea of using chemical reactions to measure time has been proposed before, for example, using lead chromate,[29] which records a lead ion concentration in water over time by changes in color. Also, the erosion of materials such as metals[30] (Fe, Mg, Mo, W, Zn), semiconductors (Si, Ge),[31] and oxides (MgO, SiO_2)[32] has been proposed to build transient electronics that disintegrate over time. In this work, we use an 80 nm thin layer of Ge contacted by two 100 nm gold contacts as an electrically readable passive timer to estimate the time spent in water. Germanium oxidizes in the presence of dissolved oxygen with the formed oxide readily dissolving in water.[23,33] This oxidation and subsequent etching process thins down the Ge film and manifests in an increasing resistance over time. After SynCell deployment and retrieval, the film resistance is an analog electric representation of how much time it has been dispersed in an aqueous solution.

https://doi.org/10.1021/acsnano.1c01259
ACS Nano 2021, 15, 8803–8812

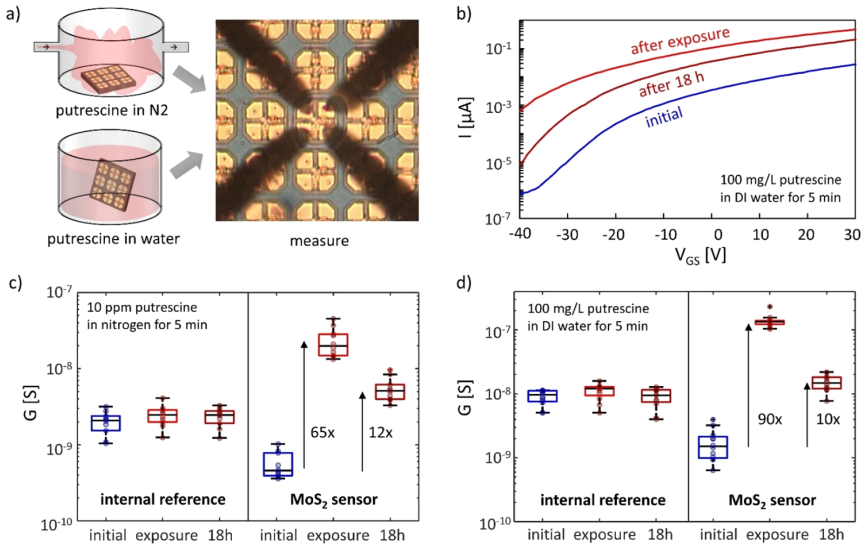

Figure 3. MoS_2-based chemical sensor characterization. (a) MoS_2 chemical sensors were exposed to putrescine in both water (100 mg/L, 5 min exposure) and nitrogen (10 ppm of putrescine in N_2, 5 min exposure, 5 min purging in N_2). (b) Transfer characteristic of a back-gated chemical sensor before and after exposure to putrescine in DI water. The negative threshold voltage shift indicates n-type doping of the MoS_2. (c) MoS_2 conductance of 10 sensors and 10 reference sensors before, right after, and 18 h after putrescine gas exposure. (d) MoS_2 conductance of 12 sensors and 12 reference sensors before, right after, and 18 h after 100 mg/L putrescine in water.

The erosion of germanium timers in water is illustrated in Figure 2a), which shows microscope images of the same device at four different times as it is slowly eroding in DI water. The water bath was kept at 60 °C to accelerate the etching (see Methods for details). The germanium close to the gold pads is eroded after 4 min. After about 16 min the entire thin film has been etched. This is consistent with previous work[34,35] that reports the accelerated etching of Ge in the presence of noble metals due to their catalytic effect. Figure 2b) shows the electrical behavior of a Ge timer in room-temperature (RT) DI water over time. The current through the timer decreases by more than 5 orders of magnitude from 40 nA to 0.17 pA at 10 V bias in the span of 15 min. Lastly, Figure 2c plots the conductance of 15 Ge timers etching in RT DI water over time. As already seen in Figure 2b), the average timer conductance exponentially drops over time and is effectively open circuit after 15 min. This is consistent with anticipated deployment times of SynCells in the minutes to hour range. The box plot shows that the conductance distribution widens after the SynCells have been in water for 5 min and then narrows again toward the end. This will introduce uncertainty when inferring the exact time spent in water based on the timer conductance. Nonetheless this method will give a rough estimation of time, especially when averaging over the timer conductance of multiple SynCells. The time span of how long it takes the timer to reach open circuit is defined by material properties, device design, and its environment. One way to modulate the time constant is by varying the germanium thickness with thicker films yielding longer etch times, as shown in the Supporting Figure S2. This allows us to tune timers for different applications.

Chemical Sensors. Chemical sensors are a key building block of the proposed SynCell platform. Here, as a proof concept, MoS_2 chemical sensors have been integrated onto SynCells to detect putrescine in water and air. MoS_2 is well documented as an excellent sensor material[36] due to its extreme surface-to-body ratio and has been used to detect gases such as ammonia and triethylamine.[17,37] Putrescine is a diamine that is generated by the decomposition of meat and fish. As a result, putrescine sensors are highly relevant in food quality monitoring.[38−40] Additionally, putrescine is indicative of cell proliferation and cell growth.[41]

The MoS_2 sensors used in this work are chemiresistors, which means they change resistance as a function of chemical exposure. We chose a $1.5 \times 8\ \mu m^2$ channel of MOCVD-grown MoS_2 (see Supporting Figure S3) with 100 nm Au contacts as sensing material. Additionally, the SynCells contain internal reference sensors, which are identical to the regular sensors, but are covered by SU-8, shielding them from the outside to monitor possible sensor drift. The MoS_2 sensors embedded in the SynCell platform are also likely sensitive to other analytes such as nitric oxide, ammonia, or mercury,[36] but optimizing sensor selectivity and sensitivity is not our goal. Eventually, functionalization layers can be applied to the MoS_2 film to make the SynCells selectively sensitive to a large variety of specific analytes and molecules, for example, prostate cancer antibodies[42] or volatile organic compounds.[43]

The SynCells were tested in either DI water or nitrogen gas (see Figure 3a)). For gas sensing, 10 ppm of putrescine in a nitrogen (N_2) carrier gas was flowed into a chamber for 5 min (see Methods). Upon exposure, the sensor conductance increases by 65 times compared to its initial value (see Figure 3c)), which compares favorably to functionalized carbon nanotube sensors[40] and is also stronger than the response reported from similar unfunctionalized MoS_2 gas sensors.[37] Eighteen hours after exposure the average channel conductance was still 12 times larger than their starting value, which highlights that the sensors retain sensing information for a period of hours, effectively behaving as 1-bit memory devices over this span. This memory function is crucial to our envisioned use cases because it allows SynCells to measure their environment for minutes to hours without requiring any

https://doi.org/10.1021/acsnano.1c01259
ACS Nano 2021, 15, 8803−8812

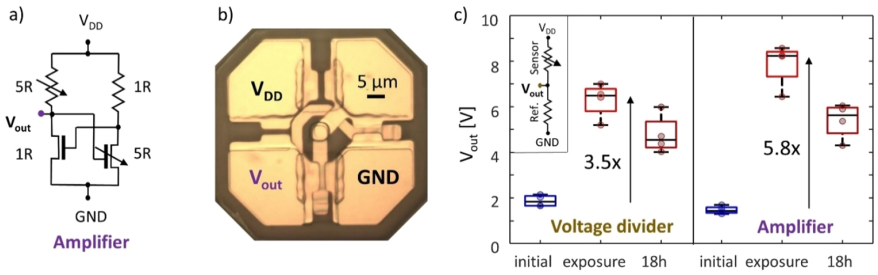

Figure 4. (a) Amplifier circuit using two transistors that feed back into each other to lower the output voltage if no exposure occurred and raise it otherwise. (b) Microscope image of an Amplifier SynCell containing the circuit shown in (a). (c) Comparison of four SynCells with passive voltage dividers consisting of a sensor and reference device (circuit see inset) as well as four Amplifier SynCells before and after exposure to 100 mg/L of putrescine in DI water for 5 min. The Amplifier SynCell increases the chemical sensor signal.

electrical power. Consequently, the sensor conductance corresponds to the integrated presence of putrescine during the measurement interval. This is an important metric in toxin detection, as their presence anywhere in the system is reason for further scrutiny. The internal reference sensors remain constant over all three measurements. It should be noted that their average conductivity is higher than in the actual sensor devices due to the SU-8 passivation inducing additional doping, as previously reported.[44]

For the liquid test, the samples were exposed to 100 mg/L of putrescine in DI water for 5 min, which is a relevant concentration for food spoilage monitoring[39,45] or for stimulating cell growth.[46] After the exposure, the samples were blow-dried and measured electrically (see Methods for details). Figure 3d shows the change in sensor conductance before and after exposure. The sensor conductance increased 90 times compared to the initial measurement and is still 10 times higher after 18 h in ambient air. The increased sensor conductance persists even after the sensors are soaked in DI water after exposure to putrescine; see Supporting Figure S4. It should also be noted that the readings of the internal reference sensors stay constant during the measurements.

The reason for the increase in conductance for both the gas and liquid exposure is an adsorption of the putrescine molecules on the MoS_2 and subsequent n-type doping of the MoS_2 channel. This is shown in Figure 3b, which plots the transfer characteristic of an unpassivated transistor before and after exposure to 100 mg/L of putrescine in DI water. The threshold voltage shifts negatively, which indicates strong n-type doping. This is consistent with earlier findings of carbon nanotube-based sensors that are p-type doped under ambient conditions and decrease in conductance when exposed to putrescine.[40] Reference tests of sensors just exposed to pure DI water or air show no significant change in sensor conductance and are shown in Supporting Figure S5.

Signal Conditioning Electronics. Besides chemical sensors and timers, we also incorporated MoS_2 transistors onto the SynCell platform for signal conditioning and amplification. MoS_2 has been studied extensively as transistor channel material in the recent past and is a promising candidate for future electronics because of its high carrier mobility, its easy integration capability, and its atomically thin nature, which is favorable for ultrascaled transistors.[47,48] In this work, we use MoS_2 transistors to amplify the chemical sensor signal to produce a low or high voltage signal depending on whether an exposure occurred. These devices can also be used to implement basic logic functions, like inverters and XOR gates.[47] The MoS_2 transistors on the SynCells are 8 μm wide and 1.5 μm long and are placed on a gold back-gate with an 800 nm thick SU-8 layer that forms the gate dielectric. SU-8 was used for this function because it is chemical resistant, mechanically flexible, and easy to pattern and has a high dielectric strength[49] (see Supporting Figure S6). While SU-8 is commonly used as a passivation layer,[44] it has only been sporadically explored as a gate dielectric in transistors.[49] The transistors have an On/Off ratio of 10^6 and exhibit a hysteresis of about 6 V. The average on-current is about 2 μA/μm, and the average mobility is 2.2 $cm^2/(V\,s)$. This is lower than state-of-the-art MoS_2 transistors[47,50−52] but still better than organic semiconductors and amorphous silicon.[53] A detailed characterization of individual transistors is provided in the Supporting Information; see Supporting Figure S7.

Figure 4a shows the amplifier design implemented in the SynCell platform using a feedback mechanism. The amplifier circuit consists of two voltage dividers where the bottom two resistors are replaced with transistors that are gated from the drain electrode of the transistor in the opposite branch. To get a differential behavior between the two voltage dividers, the left branch has a sensor at the top with the transistor underneath acting as a gate-tunable reference sensor. The right branch has a reference resistor at the top and unpassivated transistor at the bottom, also acting as a chemical sensor. As a result, the circuit lowers the output voltage if there is no chemical exposure and increases it otherwise compared to a simple voltage divider. A micrograph of this *Amplifier SynCell* is shown in Figure 4b.

Figure 4c compares the results of a passive voltage divider circuit, shown in the inset on the left, to the proposed amplifier circuit for four SynCells that have been exposed to 100 mg/L of putrescine in water for 5 min (see Methods). The amplifier circuit has a lower average output voltage of 1.4 V compared to 1.8 V on the passive voltage divider. After putrescine exposure the voltage swing of the amplifier is 66% larger compared to the voltage divider. This exemplifies that the circuit successfully amplifies the sensor signal and brings it closer to a digital high and low state of 0 and 10 V. The amplification behavior can further be improved by thinning down the gate dielectric. This will modulate the transistor resistance to a greater extent and will saturate the output close to 0 and 10 V for the unexposed and exposed state, respectively, as simulated in Supporting Figure S8.

Demonstration of Chemical Sensing and Timer Performance in a Microfluidic Channel. SynCells are small enough to sense inside spatially constrained environments that are not accessible to conventional electronic

https://doi.org/10.1021/acsnano.1c01259
ACS Nano 2021, 15, 8803−8812

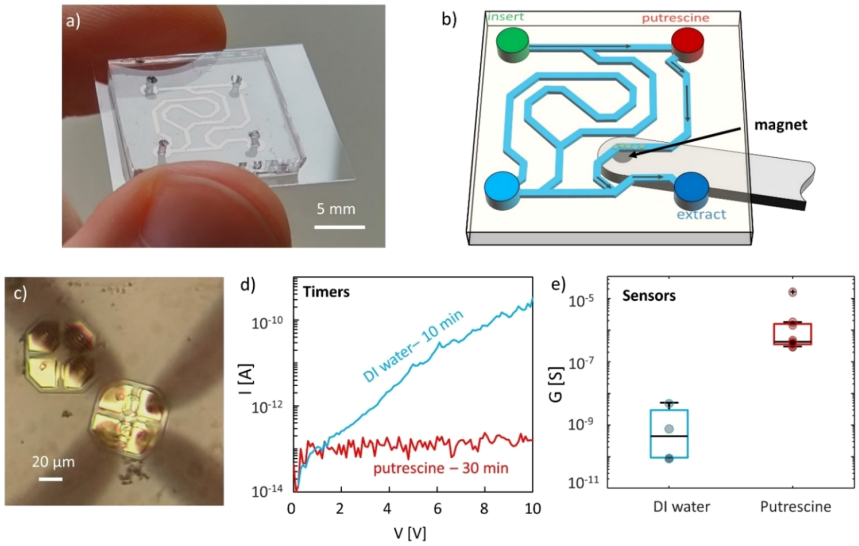

Figure 5. Sensing putrescine at a specific location in a microfluidic channel. (a) Photograph of the used microfluidic channel. (b) Test procedure for detecting putrescine in the microfluidic channel. The SynCells are inserted in the green opening at the top-left and transported with a magnet to the red top-right opening, which contains putrescine. After staying in this position for a fixed amount of time they are transported to the blue bottom-right opening, extracted, and drop-cast onto a glass slide. (c) SynCell being measured on a glass slide after it was extracted from a microfluidic channel. (d) Current−voltage curve of two timers. The first round of SynCells stayed in water for roughly 10 min, while the second round of SynCells stayed for 30 min. The Ge timer resistance supports that timing. (e) Sensor conductance of four SynCells from round 1 with just DI water in the channel and 10 SynCells from round 2 with 100 mg/L of putrescine in the red opening.

sensors. To demonstrate chemical sensing and measurement of time in constrained environments, we used SynCells to sense putrescine inside a microfluidic channel. We lead the SynCells through the channel using a magnet and detect the presence or absence of putrescine. In the future, *in situ* sensing can be enabled by integrating building blocks for wireless communication using RF[4] or light.[3]

We fabricated a maze-like channel with a channel height of 30 μm and a channel width of 500 μm, as shown in Figure 5a (see Supporting Information for fabrication details). Figure 5b illustrates the microfluidic test procedure. First the SynCells are inserted into the top left opening (green). Second, they are led to the top-right opening ("analyte opening", red) and stay there for a variable amount of time. Lastly, the SynCells are moved to the bottom-right opening (blue), where they are extracted with a pipet, cast onto a glass slide, dried (see Methods), and measured in a probe station, as depicted in Figure 5c). This procedure was carried out twice, once with DI water in the analyte opening and a total time in water of 10 min and once with putrescine (100 mg/L) in that opening and a total time in water of about 30 min. A diffusion process will distribute putrescine in the channel over time. However, even after 30 min, the concentration of putrescine is estimated to be less than 1% of the original concentration at 27% of the distance between the putrescine well and the outlet (see Supporting Figure S9).

The results for the timers and sensors are shown in Figure 5d,e), respectively. As can be seen from Figure 5d), the difference in time spent in water was clearly captured by our Ge timer. In particular, the extracted conductance of 3.3×10^{-11} S corresponds well to the previous timer characterization in Figure 3. Figure 5e) compares the sensor conductance of SynCells that went through the microfluidic channel with and without putrescine. The sensors of the SynCells exposed to putrescine are close to 1000 times more conductive than the control experiment, which successfully demonstrates the SynCells ability to sense chemicals in constrained spaces.

Videos of moving SynCells through the microfluidic channel using a magnet are shown in the Supporting Videos S1 and S2. They show that the path of the SynCells can be easily controlled by this magnetic interaction under a microscope, which should be easily applicable to other microfluidic channels. In free-flowing pipe systems, the magnetic control could also be used to capture the SynCells from the environment. Autonomous locomotion of individual SynCells may be implemented in the future, for example using air coils.[54]

CONCLUSIONS

We demonstrate a pathway to autonomous electronic microsystems (<100 μm) for sensing in constrained environments by combining electronic devices with functional materials, which lowers power consumption and minimizes system size. As a prototype, we present a 60×60 μm^2 sensing platform, the SynCell, that heterogeneously integrates MoS_2-based sensors and transistors with functional materials such as iron or germanium. The eroding germanium thin films help the SynCells to passively measure the time they spend in water. The chemical sensors detect putrescine concentrations at a level of 100 mg/L in water or 10 ppm in air, resulting in a conductance change of over 50 times. They retain this information without power over at least 18 h, thus also acting as a 1-bit memory cell. For readout, a transistor-based amplifier increases the signal of the chemical sensor by over 50%. Iron pads allow the SynCells to be positioned magnetically in tight spaces. Our experimental results show that SynCells can detect

https://doi.org/10.1021/acsnano.1c01259
ACS Nano 2021, 15, 8803−8812

putrescine at a specific location in a microfluidic channel using magnetic positioning and measuring the elapsed time. The components and concepts presented here can be useful to further lower the footprint and power consumption of microscale electronic sensor systems. In the future, such microsystems may be used to collect information from constrained spaces such as microfluidic channels or 3D-printed organs, directly probe individual cells, and even be used as printable/sprayable electronic particles for distributed sensor networks.

METHODS/EXPERIMENTAL

MoS_2 Synthesis. The synthesis of MoS_2 was conducted in a homemade MOCVD system (hot-wall type, 4-in. quartz tube reactor, 3 zone furnace). Molybdenum hexacarbonyl (MHC) and diethyl sulfide (DES) were selected as chemical precursors for Mo and S, respectively, which were injected to the quartz tube reactor as a gas phase together with N_2 and H_2. The injection of precursors and carrier gases was individually regulated with mass flow controllers (MFCs) at room temperature (25 °C). It should be noted that the injection of MHC was assisted by the N_2 carrier gas that kept the bubbler pressure 800 Torr, while DES was injected as a pure vapor form. Full-film growth of MoS_2 (monolayer yield >99%) was achieved at a constant temperature of 600 °C and a total pressure of 5 Torr. The flow rates of all precursors were kept constant during the growth: 1000 sccm N_2, 1 sccm H_2, 2 sccm MHC with N_2, and 0.1 sccm DES. After the MoS_2 growth for 2 h, the furnace was naturally cooled to room temperature with a constant flow of N_2. The growth substrate was SiO_2 (300 nm)/Si with a dimension of 3 cm × 10 cm. NaCl was placed at the upstream region of the reactor with the temperature kept at 500 °C during the growth. References 55 and 56 provide more discussion on the MOCVD process. Optical microscopy images of the as-grown MoS_2 film and an AFM scan of a transferred MoS_2 film are shown in Supporting Figure S3.

SynCell Fabrication. The SynCell fabrication protocol is described in Supporting Table S1. The top view and cross-sectional schematic of a "hybrid" SynCell as well as an optical image for each layer of the fabrication process are depicted in Supporting Table S2. In short, the fabrication process is as follows. A 4 in. bare silicon wafer is first cleaned in premixed piranha solution (Nanostrip, KMG) and 10% HCl for 5 min each to remove organic and metallic contamination, respectively. Next a 10 nm Ni/100 nm Cu film is e-beam evaporated onto the wafers as a sacrificial release layer. As bottom layer of the SynCells, SU-8 6000.5 is spin-coated on the wafer, patterned by photolithography, and hard baked, resulting in a film thickness of 800 nm. For magnetic actuation, a 10 nm Ni/100 nm Fe film is e-beam evaporated and patterned by a lift-off process with PMGI and SPR 700. Then, another layer of SU-8 6001.5 is spin-coated on the wafer, patterned by photolithography, and hard baked, resulting in a total SynCell thickness of 2000 nm. To form the electronic circuits, a 10 nm Ni/40 nm Au gate layer is deposited by electron beam (e-beam) evaporation and patterned using a lift-off process with PMGI and SPR 700. As dielectric, an 800 nm film of SU-8 is deposited by spin coating SU-8 2000.5, patterned by photolithography, and hard baked. For the passive timers, an 80 nm thick Ge film is e-beam evaporated and patterned by a lift-off process with PMGI and SPR 700. Next, the wafer is broken into 25 × 25 mm dies, which makes the MoS_2 wet transfer easier. For the transfer, MoS_2 was grown on a Si/SiO_2 substrate; see MoS_2 synthesis above. The as-grown MoS_2 film is coated with PMMA A6 950. To transfer it on the SynCell die, the PMMA/MoS_2 film is first delaminated in a beaker filled with DI water. Due to the difference in hydrophobicity between the SiO_2 and MoS_2 surface, the water penetrates at the interface detaching the PMMA/MoS_2 from the SiO_2 substrate on DI water. In a second step, the floating film of PMMA/MoS_2 is then scooped up with the SynCell chip, blow-dried for about 1 min, and left to dry overnight. The transfer process was optimized to not create wrinkles. After fully drying, the sample is baked at 150 °C for 5 min to improve the adhesion between SU-8 and MoS_2. Next, the PMMA is removed by soaking in acetone, gently rinsing with IPA, and blow-drying the sample. The MoS_2 is patterned into sensor and transistor structures by first defining mesa areas with a PGMI/SPR700 photoresist polymer mask patterned by photolithography and subsequently etching the exposed MoS_2 regions by an oxygen plasma for 3 min. The PGMI/SPR is then removed by flood exposure and a second development step. For the source and drain contacts a 100 nm film of Au is e-beam evaporated and patterned using a photolithography lift-off process. As passivation layer on top of the transistors, an 800 nm film of SU-8 is deposited by spin coating SU-8 2000.5, patterned by photolithography, and hard baked.

SynCell Release Process. The protocol to release SynCells from the substrate and measure them is described in the Supporting Table S3 and illustrated in Supporting Figures S10 and S11. In short, the finished SynCell chip is coated with an MMA 8.5 EL 11 copolymer and patterned into a mesh with 10 μm holes between the SynCells. This speeds up the undercutting. Next, the SynCell chip with MMA mesh is released in iron chloride (Transcene CE-100), which takes about 10 min. The floating film is then transferred onto a similar-sized silicon chip coated with PMMA A6, blow-dried, and baked. Subsequently, the MMA mesh is removed by a flood exposure in 220 nm DUV light and development. At this point the transferred SynCells can be electrically characterized after having gone through the entire fabrication and release process. To disperse the SynCells, the chip is immersed in acetone and the SynCells lift off within a few minutes. Afterward the solvent can be changed to isopropyl alcohol or DI water.

Microfluidic Channel Fabrication. The protocol to fabricate microfluidic channels is given in Supporting Table S4. In summary, approximately 30 μm thick SU-8 (mr-DWL 40) is spin coated on clean 2 × 2 cm pieces of SiO_2/Si and patterned by photolithography. Next, PDMS (Sylgard 184) is mixed, poured onto the molds, and baked for 2 h at 75 °C to cure the PDMS. Afterward it is bonded onto a 150 μm thick glass slide by first activating the PDMS and glass surface in an oxygen plasma and then pressing them together lightly. Last, access holes are punched with a 1.75 mm outer diameter biopsy punch.

Electric Characterization. All electric measurements where performed on a Cascade Microtech Summit 11000 AP manual probe station with DCP-HTR 10 μm diameter probe tips using an Agilent 4155 semiconductor analyzer. A standard measurement for one Syncell takes about 2−3 min.

Germanium Timer Characterization in Water. The timer characterization in water was performed as follows. SynCells were first fabricated and transferred onto a PMMA/Si carrier, as described above in SynCell Fabrication and SynCell Release Process in the Methods section. Before water testing, an initial *IV* characteristic was recorded on a probe station. Next the germanium timers were immersed for 1 min in 60 °C warm water or 5 min in 20 °C warm water. Subsequently, the chip was taken out of water and blow-dried for about 15 s with nitrogen. Afterward, they were baked for 1 min at 60 °C to remove any remaining water and were measured electrically again. This procedure was repeated 3 to 4 times to collect time-resolved changes in conductance.

Sensor Characterization in Water. The sensor characterization in water was performed as follows. The sensors were tested in pure DI water as well as DI water with 100 mg/L of putrescine dissolved in it (1,4-diaminobutane 98+% 25 g, Fisher Scientific). For a standard experiment, SynCells were lifted-off from the fabrication substrate, transferred onto PMMA/Si (see SynCell Release Process in the Methods section), and measured in their initial state. Next, the SynCell chip was submerged in either DI water or DI water with putrescine for 5 min. Subsequently, the chip was taken out of water and blow-dried for about 15 s with nitrogen. Afterward, they were baked for 5 min at 60 °C to remove any remaining water and were measured electrically again. Without the baking time some unpassivated transistors, which were used to measure the transfer characteristics as a function of chemical concentration, short-circuited at high gate bias and burned out.

https://doi.org/10.1021/acsnano.1c01259
ACS Nano 2021, 15, 8803−8812

Sensor Characterization in Nitrogen. The sensors were tested in air as well as in nitrogen with 10 ppm of putrescine (1,4-diaminobutane 98+% 25 g, Fisher Scientific). For a standard experiment, SynCells were lifted-off from the fabrication substrate, transferred onto PMMA/Si (see SynCell Release Process in the Methods section, and measured in their initial state. For the putrescine gas exposure, the SynCell chip was placed into a PTFE chamber (approximate volume 2 L) for 5 min while 10 ppm of putrescine was flowed in with 976 sccm of nitrogen as carrier gas, generated by a FlexStream base module from KIN-TEK. The putrescine dilution from the FlexStream was generated by first heating putrescine to 40 °C in a glass tube, turning it into a liquid. Nitrogen (60 sccm) was flowed through the glass tube to pick up putrescine into the gas phase. This gas stream was diluted with 976 sccm of nitrogen to dilute the putrescine concentration to 10 ppm. After exposure, the chamber was purged with 2000 sccm of pure nitrogen for 5 min. The control samples were left open in the ambient air for the same time. About 30 min passed between taking out the samples from the gas chamber and characterizing them electrically.

Microfluidic Channel Demonstration. For the sensing in a microfluidic channel, SynCells where first dispersed in water as outlined in Supporting Table S2 and illustrated in Supporting Figures S10 and S11. Once they are dispersed in water, the germanium timer starts working. After dispersion, the SynCells were first left to settle in the glass vial filled with water. Afterward about 100 μL of water and SynCell were extracted with a VWR Signature single-channel pipet (20−200 μL) with a one-time-use tip. The tip was inserted into the microfluidic channel, and the SynCells were dispersed into the 1.75 mm opening. Afterward a niobium rare earth disk-shaped magnet (1 mm diameter, 1 mm height) under the microfluidic channel was used to lead the SynCells through the microfluidic channel; see Supporting Videos S1 and S2. At the end, the SynCells were again collected with the same pipet and a new tip, drop-casted onto a glass slide, and dried for 5 min on a 60 °C hot plate. For the first experiment, no putrescine was present in the microfluidic channel and the total time from dispersion in water to collection of SynCells was about 10 min. For the second experiment, putrescine was introduced at the top-right well in the microfluidic channel (see Figure 5b). In this case, the total time from dispersion to drop-casting was 30 min, whereby the SynCells were first left in a water-filled vial for about 15 min and also were left in the putrescine well for about 5 min.

ASSOCIATED CONTENT

Supporting Information

Additional characterization of SynCells as well as a detailed process flow. Additionally, there are two supporting videos showing the manipulation of SynCells in a microfluidic channel. The Supporting Information is available free of charge at https://pubs.acs.org/doi/10.1021/acsnano.1c01259.

(MP4)
(MP4)
(PDF)

AUTHOR INFORMATION

Corresponding Author

Tomás Palacios − *Department of Electrical Engineering and Computer Science, Massachusetts Institute of Technology, Cambridge, Massachusetts 02139, United States;* orcid.org/0000-0002-2190-563X; Email: tpalacios@mit.edu

Authors

Marek Hempel − *Department of Electrical Engineering and Computer Science, Massachusetts Institute of Technology, Cambridge, Massachusetts 02139, United States;* orcid.org/0000-0002-5151-1180

Vera Schroeder − *Department of Chemistry, Massachusetts Institute of Technology, Cambridge, Massachusetts 02139, United States;* orcid.org/0000-0002-6255-4418

Chibeom Park − *Department of Chemistry, Pritzker School of Molecular Engineering, and James Franck Institute, University of Chicago, Chicago, Illinois 60637, United States;* orcid.org/0000-0003-0603-292X

Volodymyr B. Koman − *Department of Chemical Engineering, Massachusetts Institute of Technology, Cambridge, Massachusetts 02139, United States*

Mantian Xue − *Department of Electrical Engineering and Computer Science, Massachusetts Institute of Technology, Cambridge, Massachusetts 02139, United States*

Elaine McVay − *Department of Electrical Engineering and Computer Science, Massachusetts Institute of Technology, Cambridge, Massachusetts 02139, United States;* orcid.org/0000-0002-6572-3432

Sarah Spector − *Department of Electrical Engineering and Computer Science, Massachusetts Institute of Technology, Cambridge, Massachusetts 02139, United States*

Madan Dubey − *Sensors and Electron Devices Directorate, U.S. Army Research Laboratory, Adelphi, Maryland 20783, United States*

Michael S. Strano − *Department of Chemical Engineering, Massachusetts Institute of Technology, Cambridge, Massachusetts 02139, United States;* orcid.org/0000-0003-2944-808X

Jiwoong Park − *Department of Chemistry, Pritzker School of Molecular Engineering, and James Franck Institute, University of Chicago, Chicago, Illinois 60637, United States*

Jing Kong − *Department of Electrical Engineering and Computer Science, Massachusetts Institute of Technology, Cambridge, Massachusetts 02139, United States;* orcid.org/0000-0003-0551-1208

Complete contact information is available at: https://pubs.acs.org/10.1021/acsnano.1c01259

Notes

The authors declare no competing financial interest.

ACKNOWLEDGMENTS

The authors acknowledge financial support from the Air Force Office of Scientific Research under the MURI-FATE programs (Grant Nos. FA9550-15-1-0514 and FA9550-16-1-0031) as well as partial support by the ARO project W911NF-19-10372 (award title: Optical Communication with Synthetic Cells). V.S. was supported by the KAUST sensor project CRF2015-SENSORS-2719. This work was carried out in part using MIT's Microsystems Technology Laboratories and MIT.nano.

REFERENCES

(1) Nge, P. N.; Rogers, C. I.; Woolley, A. T. Advances in Microfluidic Materials, Functions, Integration, and Applications. *Chem. Rev.* **2013**, *113* (4), 2550−2583.

(2) Cui, P.; Wang, S. Application of Microfluidic Chip Technology in Pharmaceutical Analysis: A Review. *J. Pharm. Anal.* **2019**, *9* (4), 238−247.

(3) Lee, S.; Cortese, A. J.; Gandhi, A. P.; Agger, E. R.; McEuen, P. L.; Molnar, A. C. A 250 μm × 57 μm Microscale Opto-Electronically Transduced Electrodes (MOTEs) for Neural Recording. *IEEE Trans. Biomed. Circuits Syst.* **2018**, *12* (6), 1256−1266.

(4) O'Driscoll, S.; Korhummel, S.; Cong, P.; Zou, Y.; Sankaragomathi, K.; Zhu, J.; Deyle, T.; Dastgheib, A.; Lu, B.;

Tierney, M.; Shao, J.; Gutierrez, C.; Jones, S.; Yao, H. A 200μm × 200μm × 100μm, 63nW, 2.4 GHz Injectable Fully-Monolithic Wireless Bio-Sensing System. In *2017 IEEE Radio Frequency Integrated Circuits Symposium (RFIC)*; IEEE, 2017; pp 256−259; DOI: 10.1109/RFIC.2017.7969066.

(5) Biederman, W.; Yeager, D. J.; Narevsky, N.; Koralek, A. C.; Carmena, J. M.; Alon, E.; Rabaey, J. M. A Fully-Integrated, Miniaturized (0.125 mm^2) 10.5 MW Wireless Neural Sensor. *IEEE J. Solid-State Circuits* **2013**, *48* (4), 960−970.

(6) Georgiou, S. C.; Georgiou, P.; Body Dust: Miniaturized Highly-Integrated Low Power Sensing for Remotely Powered Drinkable CMOS Bioelectronics. *ArXiv* 1805.05840, 2018; https://arxiv.org/abs/1805.05840 (accessed Apr 27, 2021).

(7) Fekete, Z. Recent Advances in Silicon-Based Neural Microelectrodes and Microsystems: A Review. *Sens. Actuators, B* **2015**, *215*, 300−315.

(8) Modena, M. M.; Chawla, K.; Misun, P. M.; Hierlemann, A. Smart Cell Culture Systems: Integration of Sensors and Actuators into Microphysiological Systems. *ACS Chem. Biol.* **2018**, *13* (7), 1767−1784.

(9) Pister, K. S. J. Smart Dust https://eecs.berkeley.edu/∼pister/SmartDust/SmartDustBAA97-43-Abstract.pdf (accessed Apr 21, 2021).

(10) Warneke, B.; Last, M.; Liebowitz, B.; Pister, K. S. J. Smart Dust: Communicating with a Cubic-Millimeter Computer. *Computer (Long. Beach. Calif).* **2001**, *34* (1), 44−51.

(11) Usami, M. An Ultra-Small RFID Chip: μ-Chip. *In Proceedings of 2004 IEEE Asia-Pacific Conference on Advanced System Integrated Circuits* **2004**, 2−5.

(12) Chen, G.; Ghaed, H.; Haque, R.; Wieckowski, M.; Kim, Y.; Kim, G.; Fick, D.; Kim, D.; Seok, M.; Wise, K.; Blaauw, D.; Sylvester, D. A Cubic-Millimeter Energy-Autonomous Wireless Intraocular Pressure Monitor. *In 2011 IEEE International Solid-State Circuits Conference* **2011**, 310−312.

(13) Lee, Y.; Bang, S.; Lee, I.; Kim, Y.; Kim, G.; Ghaed, M. H.; Pannuto, P.; Dutta, P.; Sylvester, D.; Blaauw, D. A Modular 1 mm^3 Die-Stacked Sensing Platform with Low Power I2C Inter-Die Communication and Multi-Modal Energy Harvesting. *IEEE J. Solid-State Circuits* **2013**, *48* (1), 229−243.

(14) Seo, D.; Neely, R. M.; Shen, K.; Singhal, U.; Alon, E.; Rabaey, J. M.; Carmena, J. M.; Maharbiz, M. M. Wireless Recording in the Peripheral Nervous System with Ultrasonic Neural Dust. *Neuron* **2016**, *91* (3), 529−539.

(15) Funke, D. A.; Mayr, P.; Straczek, L.; McCaskill, J. S.; Oehm, J.; Pohl, N. A 200 μm by 100 μm Smart Dust System with an Average Current Consumption of 1.3 NA. In *2016 IEEE International Conference on Electronics, Circuits and Systems (ICECS)*; IEEE, 2016; pp 512−515; DOI: 10.1109/ICECS.2016.7841251.

(16) Wu, X.; Lee, I.; Dong, Q.; Yang, K.; Kim, D.; Wang, J.; Peng, Y.; Zhang, Y.; Saliganc, M.; Yasuda, M.; Kumeno, K.; Ohno, F.; Miyoshi, S.; Kawaminami, M.; Sylvester, D.; Blaauw, D. A 0.04 mm^3 16nW Wireless and Batteryless Sensor System with Integrated Cortex-M0+ Processor and Optical Communication for Cellular Temperature Measurement. In *2018 IEEE Symposium on VLSI Circuits*; IEEE, 2018; pp 191−192; DOI: 10.1109/VLSIC.2018.8502391.

(17) Koman, V. B.; Liu, P.; Kozawa, D.; Liu, A. T.; Cottrill, A. L.; Son, Y.; Lebron, J. A.; Strano, M. S. Colloidal Nanoelectronic State Machines Based on 2D Materials for Aerosolizable Electronics. *Nat. Nanotechnol.* **2018**, *13* (9), 819−827.

(18) Baba, T. Photonic and Iontronic Sensing in GaInAsP Semiconductor Photonic Crystal Nanolasers. *Photonics* **2019**, *6* (2), 65.

(19) Gómez-Martínez, R.; Hernández-Pinto, A. M.; Duch, M.; Vázquez, P.; Zinoviev, K.; de la Rosa, E. J.; Esteve, J.; Suárez, T.; Plaza, J. A. Silicon Chips Detect Intracellular Pressure Changes in Living Cells. *Nat. Nanotechnol.* **2013**, *8* (7), 517.

(20) Hu, X.; Aggarwal, K.; Yang, M. X.; Parizi, K. B.; Xu, X.; Akin, D.; Poon, A. S. Y.; Wong, H.-S. P. Micrometer-Scale Magnetic-Resonance-Coupled Radio-Frequency Identification and Transceivers for Wireless Sensors in Cells. *Phys. Rev. Appl.* **2017**, *8* (1), 014031.

(21) Soto, F.; Wang, J.; Ahmed, R.; Demirci, U. Medical Micro/Nanorobots in Precision Medicine. *Advanced Science* **2020**, *7* (21), 2002203.

(22) Lallement, G.; Abouzeid, F.; Cochet, M.; Daveau, J. M.; Roche, P.; Autran, J. L. A 2.7pJ/Cycle 16 MHz SoC with 4.3nW Power-Off ARM Cortex-M0+ Core in 28nm FD-SOI. In *ESSCIRC 2017 - 43rd IEEE European Solid State Circuits Conference*; Institute of Electrical and Electronics Engineers Inc., 2017; pp 153−162; DOI: 10.1109/ESSCIRC.2017.8094550.

(23) Sioncke, S.; Brunco, D. P.; Meuris, M.; Uwamahoro, O.; Van Steenbergen, J.; Vrancken, E.; Heyns, M. M. Etch Rates of Ge, GaAs and InGaAs in Acids, Bases and Peroxide Based Mixtures. *ECS Trans.* **2009**, *16* (10), 451−460.

(24) Schuerle, S.; Soleimany, A. P.; Yeh, T.; Anand, G. M.; Häberli, M.; Fleming, H. E.; Mirkhani, N.; Qiu, F.; Hauert, S.; Wang, X.; Nelson, B. J.; Bhatia, S. N. Synthetic and Living Micropropellers for Convection-Enhanced Nanoparticle Transport. *Sci. Adv.* **2019**, *5* (4), No. eaav4803.

(25) Nemani, K. V.; Moodie, K. L.; Brennick, J. B.; Su, A.; Gimi, B. *In Vitro* and *in Vivo* Evaluation of SU-8 Biocompatibility. *Mater. Sci. Eng., C* **2013**, *33* (7), 4453−4459.

(26) Feng, R.; Farris, R. J. Influence of Processing Conditions on the Thermal and Mechanical Properties of SU8 Negative Photoresist Coatings. *J. Micromechanics Microengineering* **2003**, *13* (1), 80−88.

(27) Kang, S. K.; Park, G.; Kim, K.; Hwang, S. W.; Cheng, H.; Shin, J.; Chung, S.; Kim, M.; Yin, L.; Lee, J. C.; Lee, K. M.; Rogers, J. A. Dissolution Chemistry and Biocompatibility of Silicon- and Germanium-Based Semiconductors for Transient Electronics. *ACS Appl. Mater. Interfaces* **2015**, *7* (17), 9297−9305.

(28) Dobrzyński, D.; Boguszewska-Czubara, A.; Sugimori, K. Hydrogeochemical and Biomedical Insights into Germanium Potential of Curative Waters: A Case Study of Health Resorts in the Sudetes Mountains (Poland). *Environ. Geochem. Health* **2018**, *40* (4), 1355−1375.

(29) Gerber, L. C.; Rosenfeld, L.; Chen, Y.; Tang, S. K. Y. Time Capsule: An Autonomous Sensor and Recorder Based on Diffusion-Reaction. *Lab Chip* **2014**, *14* (22), 4324−4328.

(30) Yin, L.; Cheng, H.; Mao, S.; Haasch, R.; Liu, Y.; Xie, X.; Hwang, S.-W.; Jain, H.; Kang, S.-K.; Su, Y.; Li, R.; Huang, Y.; Rogers, J. A. Dissolvable Metals for Transient Electronics. *Adv. Funct. Mater.* **2014**, *24* (5), 645−658.

(31) Kang, S.-K. K.; Park, G.; Kim, K.; Hwang, S.-W. W.; Cheng, H. Y.; Shin, J. H.; Chung, S. J.; Kim, M.; Yin, L.; Lee, J. C.; Lee, K.-M. M.; Rogers, J. A. Dissolution Chemistry and Biocompatibility of Silicon- and Germanium-Based Semiconductors for Transient Electronics. *ACS Appl. Mater. Interfaces* **2015**, *7* (17), 9297−9305.

(32) Hwang, S.-W.; Tao, H.; Kim, D.-H.; Cheng, H.; Song, J.-K.; Rill, E.; Brenckle, M. A.; Panilaitis, B.; Won, S. M.; Kim, Y.-S.; Song, Y. M.; Yu, K. J.; Ameen, A.; Li, R.; Su, Y.; Yang, M.; Kaplan, D. L.; Zakin, M. R.; Slepian, M. J.; Huang, Y. J. A.; et al. A Physically Transient Form of Silicon Electronics. *Science (Washington, DC, U. S.)* **2012**, *337* (6102), 1640.

(33) Harvey, W. W.; Gatos, H. C. The Reaction of Germanium with Aqueous Solutions: I. Dissolution Kinetics in Water Containing Dissolved Oxygen. *J. Electrochem. Soc.* **1958**, *105* (11), 654−660.

(34) Kawase, T.; Mura, A.; Dei, K.; Nishitani, K.; Kawai, K.; Uchikoshi, J.; Morita, M.; Arima, K. Metal-Assisted Chemical Etching of Ge(100) Surfaces in Water toward Nanoscale Patterning. *Nanoscale Res. Lett.* **2013**, *8* (1), 151.

(35) Kawase, T.; Mura, A.; Nishitani, K.; Kawai, Y.; Kawai, K.; Uchikoshi, J.; Morita, M.; Arima, K. Catalytic Behavior of Metallic Particles in Anisotropic Etching of Ge(100) Surfaces in Water Mediated by Dissolved Oxygen. *J. Appl. Phys.* **2012**, *111* (12), 126102.

(36) Anichini, C.; Czepa, W.; Pakulski, D.; Aliprandi, A.; Ciesielski, A.; Samorì, P. Chemical Sensing with 2D Materials. *Chem. Soc. Rev.* **2018**, *47* (13), 4860−4908.

(37) Perkins, F. K.; Friedman, A. L.; Cobas, E.; Campbell, P. M.; Jernigan, G. G.; Jonker, B. T. Chemical Vapor Sensing with Monolayer MoS2. *Nano Lett.* **2013**, *13* (2), 668−673.
(38) Gardini, F.; Özogul, Y.; Suzzi, G.; Tabanelli, G.; Özogul, F. Technological Factors Affecting Biogenic Amine Content in Foods: A Review. *Front. Microbiol.* **2016**, *7*, 1218.
(39) Edwards, R. A.; Dainty, R. H.; Hibbard, C. M. Putrescine and Cadaverine Formation in Vacuum Packed Beef. *J. Appl. Bacteriol.* **1985**, *58* (1), 13−19.
(40) Liu, S. F.; Petty, A. R.; Sazama, G. T.; Swager, T. M. Single-Walled Carbon Nanotube/Metalloporphyrin Composites for the Chemiresistive Detection of Amines and Meat Spoilage. *Angew. Chem., Int. Ed.* **2015**, *54* (22), 6554−6557.
(41) Chen, X.-F.; Xia, X.-X.; Lee, S. Y.; Qian, Z.-G. Engineering Tunable Biosensors for Monitoring Putrescine in Escherichia Coli. *Biotechnol. Bioeng.* **2018**, *115* (4), 1014−1027.
(42) Lee, J.; Dak, P.; Lee, Y.; Park, H.; Choi, W.; Alam, M. A.; Kim, S. Two-Dimensional Layered MoS_2 Biosensors Enable Highly Sensitive Detection of Biomolecules. *Sci. Rep.* **2015**, *4*, 7352.
(43) Kim, J.-S. S.; Yoo, H.-W. W.; Choi, H. O.; Jung, H.-T. T. Tunable Volatile Organic Compounds Sensor by Using Thiolated Ligand Conjugation on MoS2. *Nano Lett.* **2014**, *14* (10), 5941−5947.
(44) Kung, Y.-C.; Hosseini, N.; Dumcenco, D.; Fantner, G. E.; Kis, A. Air and Water-Stable *n*-Type Doping and Encapsulation of Flexible MoS2 Devices with SU8. *Adv. Electron. Mater.* **2019**, *5* (1), 1800492.
(45) Rauscher-Gabernig, E.; Gabernig, R.; Brueller, W.; Grossgut, R.; Bauer, F.; Paulsen, P. Dietary Exposure Assessment of Putrescine and Cadaverine and Derivation of Tolerable Levels in Selected Foods Consumed in Austria. *Eur. Food Res. Technol.* **2012**, *235* (2), 209−220.
(46) Farriol, M.; Segovia-Silvestre, T.; Castellanos, J. M.; Venereo, Y.; Orta, X. Role of Putrescine in Cell Proliferation in a Colon Carcinoma Cell Line. *Nutrition* **2001**, *17* (11), 934−938.
(47) Yu, L.; El-Damak, D.; Radhakrishna, U.; Ling, X.; Zubair, A.; Lin, Y.; Zhang, Y.; Chuang, M.-H.; Lee, Y.-H.; Antoniadis, D.; Kong, J.; Chandrakasan, A.; Palacios, T. Design, Modeling, and Fabrication of Chemical Vapor Deposition Grown MoS_2 Circuits with E-Mode FETs for Large-Area Electronics. *Nano Lett.* **2016**, *16* (10), 6349−6356.
(48) Zeng, M.; Xiao, Y.; Liu, J.; Yang, K.; Fu, L. Exploring Two-Dimensional Materials toward the Next-Generation Circuits: From Monomer Design to Assembly Control. *Chem. Rev.* **2018**, *118* (13), 6236−6296.
(49) Tetzner, K.; Bose, R. I.; Bock, K. Organic Field-Effect Transistors Based on a Liquid-Crystalline Polymeric Semiconductor Using SU-8 Gate Dielectrics on Flexible Substrates. *Materials* **2014**, *7* (11), 7226−7242.
(50) Chang, H.-Y.; Zhu, W.; Akinwande, D. On the Mobility and Contact Resistance Evaluation for Transistors Based on MoS_2 or Two-Dimensional Semiconducting Atomic Crystals. *Appl. Phys. Lett.* **2014**, *104* (11), 113504.
(51) Choi, M.; Park, Y. J.; Sharma, B. K.; Bae, S.-R.; Kim, S. Y.; Ahn, J.-H. Flexible Active-Matrix Organic Light-Emitting Diode Display Enabled by MoS2 Thin-Film Transistor. *Sci. Adv.* **2018**, *4* (4), No. eaas8721.
(52) Chang, H.-Y.; Yogeesh, M. N.; Ghosh, R.; Rai, A.; Sanne, A.; Yang, S.; Lu, N.; Banerjee, S. K.; Akinwande, D. Large-Area Monolayer MoS_2 for Flexible Low-Power RF Nanoelectronics in the GHz Regime. *Adv. Mater.* **2016**, *28* (9), 1818−1823.
(53) Street, R. A. Thin-Film Transistors. *Adv. Mater.* **2009**, *21* (20), 2007−2022.
(54) Xu, T.; Yu, J.; Yan, X.; Choi, H.; Zhang, L. Magnetic Actuation Based Motion Control for Microrobots: An Overview. *Micromachines* **2015**, *6* (9), 1346−1364.
(55) Kang, K.; Xie, S.; Huang, L.; Han, Y.; Huang, P. Y.; Mak, K. F.; Kim, C.-J.; Muller, D.; Park, J. High-Mobility Three-Atom-Thick Semiconducting Films with Wafer-Scale Homogeneity. *Nature* **2015**, *520* (7549), 656.
(56) Xie, S.; Tu, L.; Han, Y.; Huang, L.; Kang, K.; Lao, K. U.; Poddar, P.; Park, C.; Muller, D. A.; DiStasio, R. A.; Park, J. Coherent, Atomically Thin Transition-Metal Dichalcogenide Superlattices with Engineered Strain. *Science (Washington, DC, U. S.)* **2018**, *359* (6380), 1131.

https://doi.org/10.1021/acsnano.1c01259
ACS Nano 2021, 15, 8803−8812